PHILOSOPHICAL TRANSACTIONS OF THE ROYAL SOCIETY A

rsta.royalsocietypublishing.org

Research

Cite this article: Lozovatsky ID, Fernando HJS. 2013 Mixing efficiency in natural flows. Phil Trans R Soc A 371: 20120213. http://dx.doi.org/10.1098/rsta.2012.0213

One contribution of 13 to a Theme Issue 'Turbulent mixing and beyond: non-equilibrium processes from atomistic to astrophysical scales I'.

Subject Areas:
oceanography, limnology, atmospheric science

Keywords:
mixing efficiency, turbulence, stable stratification, shear instability

Author for correspondence:
I. D. Lozovatsky
e-mail: i.lozovatsky@nd.edu

Royal Society Publishing
Informing the science of the future

Mixing efficiency in natural flows

I. D. Lozovatsky[1] and H. J. S. Fernando[1,2]

[1]Environmental Fluid Dynamics Laboratories, Department of Civil Engineering and Geological Sciences, and [2]Department of Aerospace and Mechanical Engineering, University of Notre Dame, Notre Dame, IN 46556, USA

It is argued that the mixing efficiency of naturally occurring stratified shear flows, $\gamma = Rf/(1-Rf)$, where Rf is the flux Richardson number, is dependent on at least two governing parameters: the gradient Richardson number Ri and the buoyancy Reynolds number $Re_b = \varepsilon/\nu N^2$. It is found that, in the range approximately $0.03 < Ri < 0.4$, which spans $10^4 < Re_b < 10^6$, the mixing efficiency obtained via direct measurements of fluxes and property gradients in the stable atmospheric boundary layer and homogeneous/stationary balance equations of turbulent kinetic energy (TKE) is nominally similar to that evaluated using the scalar balance equations. Outside these Ri and Re_b ranges, the commonly used flux-estimation methodology based on homogeneity and stationarity of TKE equations breaks down (e.g. buoyancy effects are unimportant, energy flux divergence is significant or flow is non-stationary). In a wide range, $0.002 < Ri < 1$, the mixing efficiency increases with Ri, but decreases with Re_b. When Ri is in the proximity of $Ri_{cr} \sim 0.1$–0.25, γ can be considered a constant $\gamma \approx 0.16$–0.2. The results shed light on the wide variability of γ noted in previous studies.

1. Introduction

The specification of eddy viscosity and diffusivities remains a central problem in developing predictive models for oceans, lakes and the atmosphere. For stably stratified flows, the vertical diffusivities can be defined in terms of vertical momentum ($\overline{u'w'}$, $\overline{v'w'}$) and buoyancy ($\overline{w'b'}$) or temperature ($\overline{w'T'}$) fluxes as

$$K_U = -\frac{\overline{u'w'}}{\partial U/\partial z} \quad \text{or} \quad K_V = -\frac{\overline{v'w'}}{\partial V/\partial z} \tag{1.1}$$

and

$$K_T = -\frac{\overline{T'w'}}{\partial \tilde{T}/\partial z}, \tag{1.2}$$

where $K_M \equiv K_U = K_V$ and K_T are the eddy viscosity and diffusivity, respectively, and their ratio $Pr_{tr} = K_M/K_T$ is the turbulent Prandtl number [1]. When temperature T is the major contributor to density ρ, as in dry atmosphere, freshwater lakes and some marine environs, the buoyancy fluctuations become $b' = -g(\rho - \rho_o)/\rho_o = -g\rho'/\rho_o \approx \alpha g T'$, and K_T can be interpreted as the mass diffusivity. Here, g is the gravity, ρ_o the reference density and α the thermal expansion coefficient. The instantaneous velocities (u, v, w) in the (x, y, z) directions are written in the usual forms $u = U + u'$, $v = V + v'$, $w = W + w'$, the temperature $T = \tilde{T} + T'$ and the density $\rho = \tilde{\rho} + \rho'$, where U, V, W, $\tilde{T}$ and $\tilde{\rho}$ represent the mean and the primes are the fluctuations. In the atmosphere, sonic anemometers and gradient measurements allow direct evaluation of K_M and K_T from (1.1) and (1.2) by turbulent fluxes (using covariance calculation) and the gradients of temperature and velocity components at a suitable vertical separation. Here, the linear overbar stands for averaging over specific time segments (assuming Taylor frozen turbulence hypothesis). In oceans and other water bodies, however, the measurement of fluxes still remains a technical challenge, and eddy diffusivities are obtained either indirectly via local microstructure measurements or directly by tracer dispersion observations over large space–time domains. In the former, the simplified equations for the budget of turbulent kinetic energy (TKE) $q^2 = 1/2(\overline{u'^2} + \overline{v'^2} + \overline{w'^2})$ and turbulent thermal variance $\Theta^2 = 1/2\overline{T'^2}$,

$$\frac{\partial q^2}{\partial t} = P - B - \varepsilon \tag{1.3}$$

and

$$\frac{\partial \Theta^2}{\partial t} = -\overline{w'T'}\frac{\partial \tilde{T}}{\partial z} - \frac{1}{2}\chi, \tag{1.4}$$

are used with the assumption of homogeneity (neglecting advection and diffusion of q^2 and Θ^2), where $P = -((\overline{u'w'}(\partial U/\partial z) + \overline{v'w'}(\partial V/\partial z))$ is the shear production of TKE and $B = -\overline{b'w'}$ is the buoyancy flux [1]. Here, mixing is assumed to be internal; that is, TKE is produced and approximately balanced locally *vis-à-vis* external mixing where the energy flux divergence and advective terms transport turbulence, which is generated elsewhere, to the mixing location [2]. Here,

$$\varepsilon = \frac{15}{4}\nu\left[\overline{\left(\frac{\partial u'}{\partial z}\right)^2} + \overline{\left(\frac{\partial v'}{\partial z}\right)^2}\right] \quad \text{and} \quad \chi = 6D\overline{\left(\frac{\partial T'}{\partial z}\right)^2} \tag{1.5}$$

are the dissipation rates of $q^2$and Θ^2 in isotropic approximation, and ν and D are the molecular viscosity and diffusivity, respectively. As mentioned previously, ε and χ in natural waters are estimated using microstructure profiling measurements [3–8] as well as acoustic Doppler current profiler and acoustic Doppler velocimeter records [9–12].

Defining traditional flux Richardson number as [1]

$$Rf = \frac{B}{P}, \tag{1.6}$$

or using a generalized definition of Rf for non-stationary and inhomogeneous turbulence [13],

$$Rf \equiv Rf_{II} = \frac{B}{\varepsilon + B}, \tag{1.6a}$$

where the denominator accounts for all local and non-local sources of the TKE production, and introducing the mixing efficiency [14]

$$\gamma \equiv \frac{B}{\varepsilon} = \frac{Rf}{1 - Rf}, \tag{1.7}$$

it is possible to write the stationary balance of TKE using equations (1.3) and (1.2) as

$$K_T = \gamma\frac{\varepsilon}{N^2}, \tag{1.8}$$

or in non-dimensional form,

$$R_m = \gamma Re_b, \tag{1.9}$$

Table 1. Various methods of evaluation the diffusivity K_T and mixing efficiency γ using measurements of temperature $\overline{w'T'}$ and buoyancy $B = -\overline{b'w'}$ fluxes and corresponding gradients $\partial\tilde{T}/\partial z$ and N^2 as well as the turbulent kinetic energy ε and temperature χ dissipation rates.

method/parameter	K_T	$\gamma = B/\varepsilon$
indirect evaluation of γ via χ	$K_T \equiv K_\chi = \chi/2(\partial\tilde{T}/\partial z)^2$ (1.12)	$K_\chi/\nu = R_{m\chi} = \gamma_\chi Re_b$ (1.9) and (1.10*b*)
evaluation of γ (using flux measurements of K_T)	$K_T = -\overline{w'T'}/\partial\tilde{T}/\partial z \equiv K_f$ (1.2)	$K_f/\nu = R_{mf} = \gamma_f Re_b$ (1.9) and (1.10*a*)
direct evaluation of γ (measurements of fluxes and dissipation)	—	$\gamma \equiv B/\varepsilon = Rf/1 - Rf$ (1.7) and $Rf_{II} = B/\varepsilon + B$ (1.6*a*)

where

$$R_m = \frac{K_T}{\nu} \tag{1.10}$$

is the mixing Reynolds number. Note that (1.6*a*) is equivalent to (1.6) if pure internal mixing is occurring, that is shear-produced turbulence is dissipating locally and consumed for buoyancy flux. For ocean mixing, Osborn [14] suggested $Rf \leq 0.17$, which gives an upper bound for K_T in (1.8) with $\gamma \approx 0.2$.

For the case where the temperature flux and gradients are measured directly $K_f \equiv K_T$, the mixing Reynolds number (1.10) becomes

$$R_{mf} = \frac{K_f}{\nu}, \tag{1.10a}$$

and the buoyancy Reynolds number is given by

$$Re_b = \frac{\varepsilon}{\nu N^2}, \tag{1.11}$$

where $N^2 = (g/\rho_o)\mathrm{d}\tilde{\rho}/\mathrm{d}z$ is the squared buoyancy frequency.

Conversely, following (1.2) and (1.4), the temperature diffusivity K_T for stationary turbulence can be estimated as

$$K_T \equiv K_\chi = \frac{\chi}{2(\partial\tilde{T}/\partial z)^2}, \tag{1.12}$$

where $\partial\tilde{T}/\partial z$ can be directly measured, and χ can be estimated from temperature microstructure data. The corresponding mixing Reynolds number is (cf. equation (1.10*a*))

$$R_{m\chi} = \frac{K_\chi}{\nu}, \tag{1.10b}$$

and the mixing efficiency $\gamma_\chi \equiv \gamma$ can be estimated using (1.8) and (1.12) [4], provided that the assumptions of stationarity and homogeneity are satisfied simultaneously [15]. Another approach of estimating $\gamma \equiv \gamma_f$ is the flux-based measurement of $K_T \equiv K_f$ using (1.2) and (1.8) or $\gamma \equiv \gamma_o$ using (1.7) with (1.6) or (1.6*a*), where the temperature flux is measured directly. For convenience, these are listed in table 1.

The objectives of this paper are (i) to compare the mixing efficiencies γ_χ and γ_f calculated by the two methods and (ii) to discuss the dependence of mixing efficiency on Ri and Re_b. The canonical flow type of interest here is the stratified shear flow that is common in oceans, lakes and the atmosphere. We will use data taken in the atmospheric nocturnal boundary layer at very high Reynolds numbers.

The present work is particularly helpful in delving into the variability of γ and therefore Rf observed in different studies that have employed a variety of techniques by analysing mixing mechanisms [15–17]. In the laboratory, Linden [18], Rohr *et al.* [19], Rohr & Van Atta [20] and

Monti *et al.* [21], among others, have used non-stationary turbulence, whereas Strang & Fernando [22] and McEwan [23] used stationary or quasi-stationary flows, yielding somewhat different results. Numerical studies with evolving [17,24,25] and stationary flows [26] show disparate Rf and γ behaviour. In all, past results illustrate the dependence of Rf and γ on the mixing mechanism [27], the state of evolution of mixing [21,24,25,28], the nature of forcing (internal versus external [2,29]) and even the effect of topography [30]. Results of several experimental and theoretical studies that showed a clear dependence of γ on Ri were summarized in fig. 10 of Lozovatsky *et al.* [31], and the repercussions of variable mixing efficiency are discussed in Balmforth *et al.* [32]. The notion of Phillips [33] that γ grows with Ri, reaches a maximum at some Richardson number ($0 < Ri <\sim 1$), and then decreases has been supported by laboratory experiments [18,34], measurements in a stably stratified atmospheric boundary layer [35] and used in the Goddard Institute for Space Studies (GISS) oceanographic numerical model of Canuto *et al.* [36]. Initial attempts to estimate γ from oceanic flux measurements and balance equations of q^2 and Θ^2 yielded a γ_χ that is significantly smaller than γ_f (a single depth towing measurements in a tidal front by Gargett & Moum [37]), but the mixing efficiency was confined to a narrow range (0.13–0.17) on the basis of vertical profiling through turbulent patches [38]. The authors noted a large uncertainty for γ estimates owing to technical difficulties of flux measurements in the ocean interior and a limited length of observational records.

It was our hope that the evaluations of γ from a comprehensive dataset that allows direct measurement (using γ_o and γ_f) and indirect evaluation (via γ_χ) of γ will help clarify the wide variability of mixing efficiencies reported in the literature. Furthermore, our dataset allows evaluation of γ as a function of governing variables of natural stratified sheared flows.

2. Governing parameters

Consider a stratified shear flow away from the boundaries, which is characterized by the buoyancy frequency N and mean shear $Sh = \sqrt{(\mathrm{d}U/\mathrm{d}z)^2 + (\mathrm{d}V/\mathrm{d}z)^2}$, with their length scales of variation L_N and L_{Sh}, respectively. The turbulence in the flow is specified by a characteristic velocity q, length scale l_{tr} and time scale τ. The molecular parameters involved are υ and D. Using $\varepsilon \approx q^3/l_{tr}$, the governing dimensional variables become N, Sh, ε, q, υ, D, L_N, L_{Sh} and τ, yielding the governing non-dimensional variables $Ri = N^2/Sh^2$, $Re_b = \varepsilon/\upsilon N^2$, $SN = Sh \times (q^2/\varepsilon)$, $\tau \times Sh$, l_{tr}/L_{Sh}, l_{tr}/L_N and $Pr = \upsilon/D$, where $l_{tr} \sim q^3/\varepsilon$ has been reintroduced. For slowly spatially varying flows or turbulent regions that are much smaller than L_N and L_{Sh}, the governing parameters become the gradient Richardson number Ri, buoyancy Reynolds number Re_b and Prandtl number Pr. The additional constraint is the evolution of turbulence in equilibrium with shear (whence the shear number SN becomes a constant [39]). At high Reynolds numbers, or at geophysical scales, it is possible to invoke the Reynolds number similarity, and assume that the flows are Pr independent.

If local shear production of turbulence is the dominant source of (internal) mixing with $l_{tr} = (L_{Sh}, L_N)$, the simplest stationary TKE balance $K_M Sh^2 \approx \varepsilon$ gives the following relationship between Re_b, Ri and R_m:

$$Re_b \equiv \frac{\varepsilon}{\upsilon N^2} = \frac{K_M}{\upsilon}\frac{Sh^2}{N^2} = R_m Pr_{tr} Ri^{-1}, \tag{2.1}$$

where the turbulent Prandtl number $Pr_{tr} = K_M/K_T$ itself can be a function of Ri whence Ri exceeds a critical Richardson number $Ri_{cr} \approx 0.1$–0.25 [40,41]. Conversely, Pr_{tr} tends to be close to unity for $Ri \ll Ri_{cr}$ [1,31,40,42]. Shih *et al.* [25] obtained an inverse dependence between Re_b and Ri similar to equation (2.1) (their eqn (5.1)), and also showed a relatively weak decrease in Pr_{tr} (from approx. 1 to 0.85) when Re_b increases from approximately 10 to 100. For $Re_b >\sim 100$, Pr_{tr} remained approximately constant. Although Ri and Re_b are formally independent governing parameters, but for shear-generated turbulence, they are related to each other in a specific parameter range. Nevertheless, it is important to note the external (the mean shear for Ri) and internal (the dissipation rate for Re_b) nature of these parameters in turbulent stratified flows.

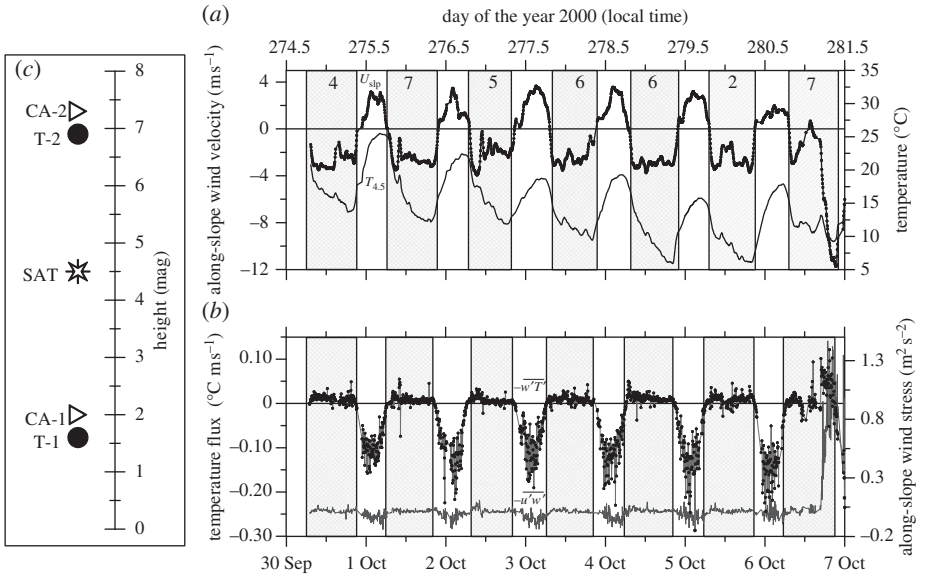

Figure 1. (*a*) Along-slope component of wind velocity U_{slp} and temperature $T_{4.5}$ at $h = 4.5$ m agl; the number of segments chosen for the calculation of mixing efficiency γ is given along the upper axis. (*b*) Temperature $\overline{w'T'}$ and momentum $-\overline{u'w'}$ fluxes at $h = 4.5$ m agl; the night-time sections of the records are shadowed in both panels. (*c*) A sketch of the observational setup at the meteorological mast: thermistors T-1 and T-2, cup anemometers CA-1 and CA-2, sonic anemometer/thermometer SAT (see text for details).

3. Observations and data processing

The data (wind velocity and sonic temperature) used in this study were obtained during the vertical transport and mixing experiment (VTMX) in Salt Lake City, Utah conducted from 30 September to 7 October 2000 (see Monti *et al.* [43] and Princevac *et al.* [44] for a general description of the experiment). A meteorological mast at a gentle (approx. 4°) mountain slope was equipped with two three-cup anemometers at heights $h = 2.0$ (CA-1) and $h = 7.3$ (CA-2) m above ground level (agl) and with two thermistor sensors at $h = 1.8$ (T-1) and $h = 6.9$ (T-2) m agl. The threshold speed of the anemometers was 0.5 m s^{-1}, with an accuracy of 1.5 per cent. The 5 min averaged data were collected to characterize the mean wind speed and air temperature. The high-frequency (10 Hz sampling rate) records of velocity components u (downslope), v (cross-slope), and w (upward) and temperature T were obtained at $h = 4.5$ m agl using a sonic anemometer/thermometer (Applied Technologies, Inc. and Metek GmbH). The resolution and accuracy of data were 0.01 and 0.05 m s^{-1}, and 0.01°C and 0.05°C, respectively. A sketch showing positions of the instruments at the mast is given in figure 1*c*. Clear skies and light synoptic winds characterized the weather conditions from 30 September until 6 October. During the last night, wind increased up to 12 m s^{-1} owing to synoptic influence. Because of the very dry atmosphere (relative humidity during the experiment did not exceed 5–8%), we did not apply a moisture correction to the sonic temperature.

The 5 min averaged records of temperature, along-slope wind velocity and vertical components of temperature and momentum fluxes at $h = 4.5$ m agl are shown in figure 1*a*,*b*. The night-time $\overline{w'T'}$ were predominantly negative as a result of the stable stratification near the ground (note 30 September 2000 is day 274 of 2006; this differs by 1 day from Monti *et al.* [43], where the leap year adjustment was not made). To obtain accurate estimates of γ, specific 20 min segments of data with almost constant fluxes and winds were selected (see a number of such segments for each night in figure 1*a*). Note that the homogeneity and stationarity of flow at specified segments were confirmed by comparing (1.6) and (1.6*a*). An example of $d\tilde{T}/dz$, $|Sh|$ and

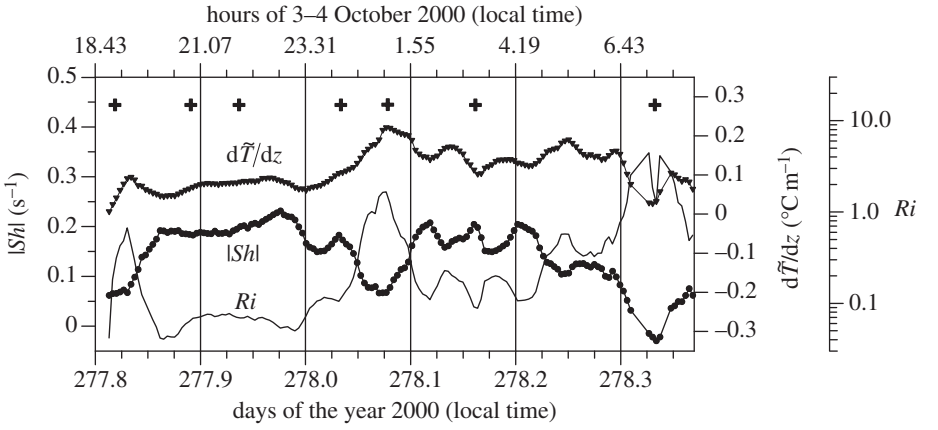

Figure 2. The gradient Richardson number *Ri*, the magnitude of mean shear $|Sh|$ and the gradient of mean temperature $\mathrm{d}\tilde{T}/\mathrm{d}z$ in a stably stratified nocturnal boundary layer ($h = 1.8$–6.9 m agl) on 3–4 October 2000. The 20 min segments of the records selected for the calculation of γ are shown by pluses.

Ri records during a typical night (3–4 October) is given in figure 2, with seven segments chosen for the calculation of γ. The flow was usually weakly stable at the beginning of the night ($Ri < 0.1$ in this case). At about midnight (figure 2), a local maximum of $Ri \approx 2$ was observed owing to a sharp drop of shear and a continuous increase in $\mathrm{d}\tilde{T}/\mathrm{d}z$, wherein the flow was dominated by quasi-periodic internal-wave oscillations [44]. Oscillations with longer periods of approximately 2–3 h were also observed [35] that could be attributed to global intermittency associated with periods of intense turbulence production and enhance stability. Continuous cooling of the surface and general reduction of mean shear towards the end of the night led to an increasing Richardson number. The natural meteorological variability during the observational period of seven nights allowed estimates of γ to be obtained over a wide range of *Ri* with high statistical confidence.

The mixing efficiency, as mentioned in table 1, was calculated directly using equations (1.6) or (1.6*a*) and (1.7) and equations (1.9) and (1.2) to obtain γ_o and γ_f, respectively, as well as indirectly to yield $\gamma \equiv \gamma_\chi$ (equations (1.9) and (1.12)). In order to estimate the mixing efficiency directly (i.e. γ_o in table 1), we first compare the flux Richardson numbers *Rf* and Rf_{II} defined differently for stationary (equation (1.6)) and non-stationary (equation (1.6*a*)) balances of TKE. Strong linear correlation between the two variables can be seen in figure 3 with $r^2 = 0.97$ for the best least-square linear regression $Rf_{II} = 1.1Rf$. This result suggests that statistically, Rf_{II} and *Rf* are almost identical, supporting the assumption of homogeneity and stationarity for the dataset considered. Thus, we can confidently use equation (1.6) paired with equation (1.7) to calculate mixing efficiency $\gamma_\mathrm{o} \equiv \gamma_\mathrm{f}$.

The covariance $\overline{w'T'}$ and Reynolds stresses were computed for selected 20 min segments using the direct covariance method and integrating the corresponding co-spectra (see several examples of $\omega E_{wT}(\log \omega_\mathrm{n})$ in figure 4*a*). A characteristic relative difference between the two temperature flux estimates was 11 per cent by amplitude, with 21 per cent standard deviation. The gradients of the mean temperature were taken as the finite differences between the 20 min averaged temperatures $\tilde{T}_1$ and $\tilde{T}_2$ located $\Delta h = 5.1$ m apart. The TKE and temperature dissipation rates, ε and χ, were obtained from the inertial and inertial-convective subranges of the velocity and temperature spectra

$$E_w(\kappa) = c_{kw}\varepsilon^{2/3}\kappa^{-5/3} \quad \text{and} \quad E_T(\kappa) = c_T\varepsilon^{-1/3}\chi\kappa^{-5/3}, \tag{3.1}$$

at each *i* segment, and the 20 min averaged wind velocities were used to convert the frequency spectra of w' and T' to the corresponding wavenumber spectra $E_w(\kappa)$ and $E_T(\kappa)$, where κ is the horizontal wavenumber. To ensure high quality of the dissipation estimates, only those spectra that exhibited a near-perfect $-5/3$ subrange were used with the canonical values of spectral

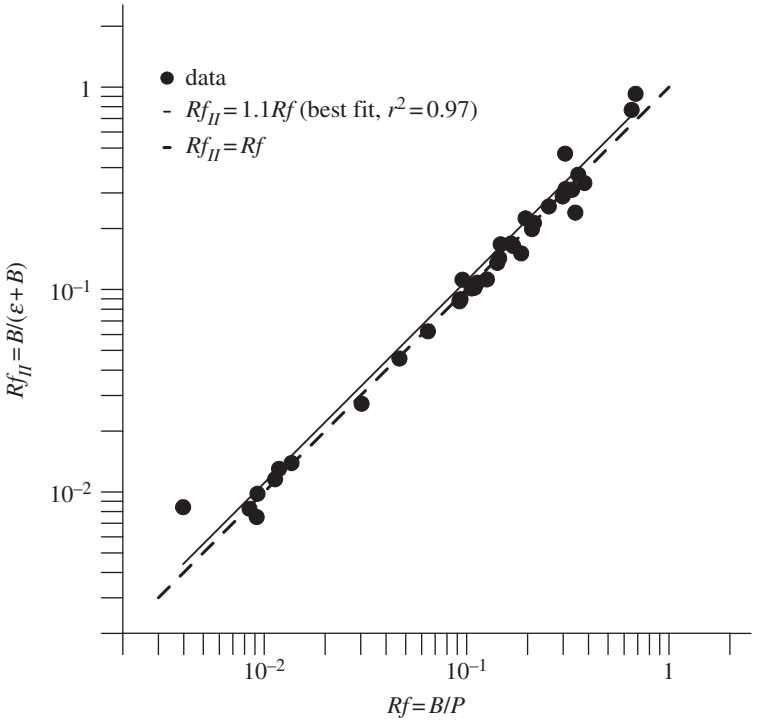

Figure 3. Correlation between the flux Richardson numbers Rf and Rf_{II} defined by equations (1.6) and (1.6*a*), respectively.

constants [45]; for the longitudinal flow component (which is u in our case), $c_{ku} = 0.52$ and for transversal components (w or v), $c_{kw} = c_{kv} = 4/3c_{ku} = 0.67$ (an example is given in figure 4*b*). A concern was the significant variation of the Obukhov–Corrsin constant c_T reported in previous studies. Sreenivasan [46] suggested $0.3 < c_T < 0.5$ with a tendency for lower c_T at higher Reynolds numbers; for that reason, $c_T = 0.3$ was used in this study. The spectra for u', v' and w' exhibited clear inertial subranges, which, as expected, were wider for $E_u(\kappa)$ and $E_v(\kappa)$ compared with $E_w(\kappa)$. At many segments, the flow was not horizontally unidirectional, thus posing problems of selecting the longitudinal and transverse directions. Therefore, the estimates of ε were made using $E_w(\kappa)$ with $c_{kw} = 0.67$ because w is the unequivocal transversal component. Two methods were used for the R_m (equation (1.10)) calculation, based on $K_T \equiv K_\mathrm{f}$ using the temperature flux and gradient measurement in (1.2), i.e. R_mf, and on $K_\mathrm{T} \equiv K_\chi$ obtained via (1.12) by estimating χ through $E_T(\kappa)$, i.e. $R_{\mathrm{m}\chi}$.

4. Dependence of mixing Reynolds numbers $R_{\mathrm{m}\chi}$ and R_mf on Ri

On the basis of arguments of §2, the diffusivities must be dependent on the gradient Richardson number Ri as well as the buoyancy Reynolds number Re_b. To explore the $R_\mathrm{m}(Ri)$ dependence, a combined plot of R_mf and $R_{\mathrm{m}\chi}$ versus Ri is shown in figure 5. Both diffusivities therein are almost identically affected by Ri following approximately $R_\mathrm{m} \sim Ri^{-3/2}$ [47]. This simple parametrization has been previously used in several numerical models [48]. The $Ri^{-3/2}$ fit is, however, applicable for a relatively narrow range of Ri.

In figure 5, R_mf flattens at a value of $R_\mathrm{mf} \approx 2.2 \times 10^3$ in the range of Ri between $Ri_\mathrm{cr} = 0.25$ and $Ri = 1$, and may even show a slightly rising tendency at larger Ri, although the latter cannot be substantiated owing to availability of few experimental points. It is, however, a possibility that the R_mf samples at $Ri > 1$ represent intermittent turbulent patches that were advected to the observational site rather than generated locally by weak vertical shear. In this case, for

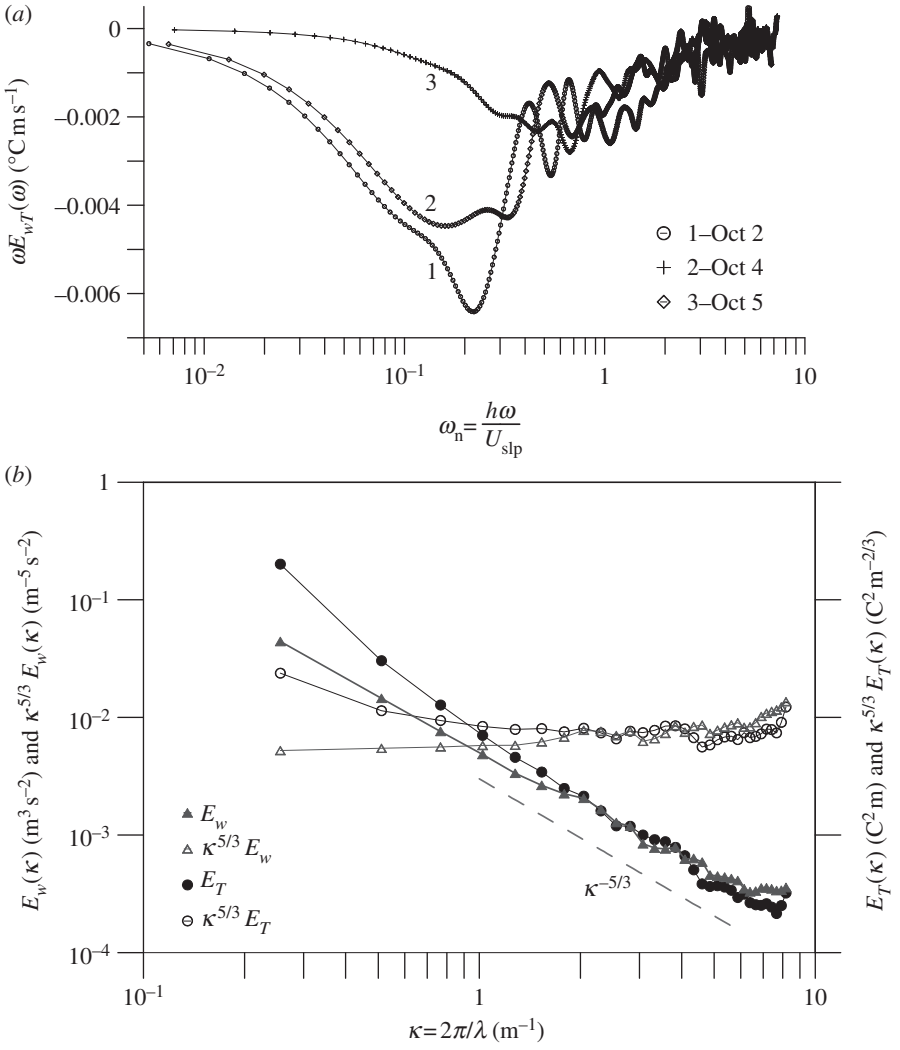

Figure 4. Examples of (*a*) co-spectra $\omega E_{wT}(\omega)$ used to obtain the integral estimates of temperature flux, where ω_n is the normalized frequency, $h = 4.5$ m. (*b*) Vertical velocity $E_w(\kappa)$ and temperature $E_T(\kappa)$ spectra (4 October 21.50–22.10) with the corresponding $\kappa^{5/3}E_w(\kappa)$ and $\kappa^{5/3}E_T(\kappa)$ that emphasize the −5/3 subranges (flat segments) used to estimate ε and χ_T.

$Ri > 1$, the local Ri does not represent the state of turbulence in the same way as that for continuous turbulence.

On the contrary, $R_{m\chi}$ continuously decreases beyond Ri_{cr}, but much slower than in the $Ri_0 - Ri_{cr}$ range, where $Ri_0 \approx 0.025$, being about an order of magnitude smaller than Ri_{cr}. For $Ri > 1$, $R_{m\chi}$ tends to a background value $R_{mb} = 600$. In the original stably stratified layer, shear-induced mixing onsets at $Ri = Ri_{cr}$, which rapidly grows until the Richardson number decreases to $Ri = Ri_0$, and then it reaches a saturation level typical of non-stratified shear flows. At $Ri < Ri_0$, R_{mf} flattens, deviating from the −3/2 power law towards $R_{mf} \sim 3 \times 10^5$, but $R_{m\chi}$ continuously increases at low Ri, reaching approximately 10^7 at $Ri \approx 10^{-3}$.

The dependences of R_{mf} and $R_{m\chi}$ on Ri evident from figure 5 can be approximated by a scaling formula

$$R_m = \frac{R_{mn}}{(1 + Ri/Ri_0)^s} + R_{mb}, \tag{4.1}$$

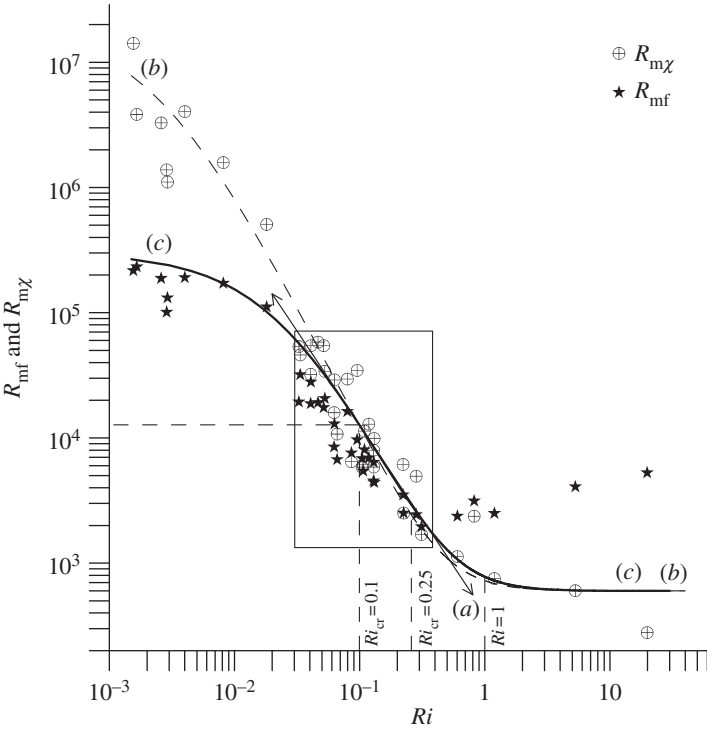

Figure 5. The mixing Reynolds numbers $R_{m\chi}$ and R_{mf} versus Ri, approximated by a simple power fit $R_m \sim Ri^{-3/2}$ (the double-arrow line (*a*)) for the box-bounded samples $0.03 < Ri < 0.4$, and by the scaling formula (4.1) with $R_{mn} = 2 \times 10^7$, $R_0 = 2.5 \times 10^{-3}$ (*b*) and $R_{mn} = 3 \times 10^5$, $R_0 = 2.5 \times 10^{-2}$. (*c*) The rectangle bounds the Ri range $0.03 < Ri < 0.4$ and the range of R_{mf} and $R_{m\chi}$ (1.5×10^3–7×10^5) for linearly correlated normalized diffusivities.

with $s = 2$. For $R_{m\chi}$, the fit is shown by the dashed line (*b*), with $R_{mn} = 2 \times 10^7$ and $R_0 = 2.5 \times 10^{-3}$, whereas the heavy line (*c*) is drawn for R_{mf} with $R_{mn} = 3 \times 10^5$ and $R_0 = 2.5 \times 10^{-2}$. The formula (4.1) belongs to the family of negative Ri power-law parametrizations of eddy viscosity and diffusivity in stably stratified flows [49–55]. Different s values have been proposed, ranging between 1 and 2.5. The value of Ri_0 in (4.1) is usually taken from 0.1 to 0.3; however, Ri_0 as low as 0.02–0.05 has been used sometimes to satisfy experimental data [31]. The fitted $Ri_0 = 2.5 \times 10^{-3}$ is much smaller than the previously suggested values, and the corresponding $R_{mn} = 2 \times 10^7$ is also unusually large. Perhaps, the presence of wall-induced turbulence in the present case may explain the anomalies; previous comparisons of (4.1) have been conducted with data taken from the thermocline or free shear flows.

This can be checked by applying the law-of-the-wall [45] test for vertical diffusivity $K_z = \kappa u_* z$, where u_* and $\kappa = 0.4$ are the friction velocity and von Karman constant, respectively. All the highest values of R_{mf} and $R_{m\chi}$ in figure 5 that correspond to the lowest $Ri < 10^{-2}$ represent seven segments of data obtained on 7 October under strong katabatic winds (the along-slope wind component varied between -10 and $-12\,\mathrm{m\,s^{-1}}$ (figure 1). A characteristic estimate of u_* for these data is approximately $1\,\mathrm{m\,s^{-1}}$ (the quadratic law formula). Thus, at $h = 4.5\,\mathrm{m}$ agl, $K_z \approx 2\,\mathrm{m^2\,s^{-1}}$, and hence $R_m \approx 1.5 \times 10^5$. This value matches well with the normalized diffusivity R_{mf} in figure 5 at the lower end of the Ri axis, but it is more than an order of magnitude smaller than the corresponding $R_{m\chi}$ for the same values of Ri. The test implies that the balance-based calculation of $R_{m\chi}$ produces unreliable estimates of the normalized diffusivity for very low Richardson numbers ($Ri < 0.03$). Probably, we can make the same conclusion about the flux-based estimates R_{mf} for high $Ri > 1$. Hence, the dependence of mixing Reynolds number R_m on Ri is best represented by equation (4.1) with $R_{mn} = 3 \times 10^5$ and $R_0 = 2.5 \times 10^{-2}$, which is shown by line (*c*) in figure 5.

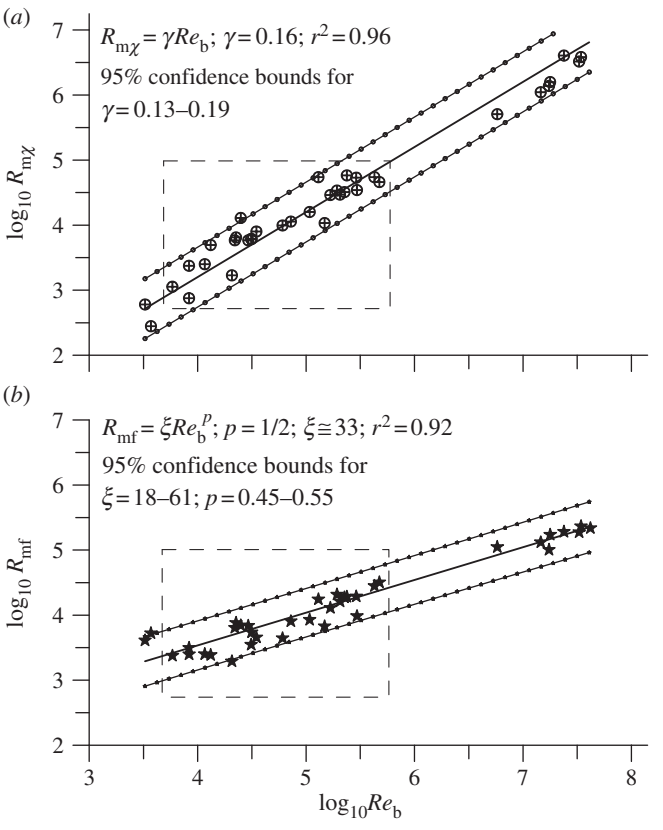

Figure 6. Regression plots between the logarithms of mixing Reynolds numbers (*a*) $R_{m\chi} = K_\chi/\nu$ and (*b*) $R_{mf} = K_f/\nu$ and the buoyancy Reynolds number $Re_b = \varepsilon/\nu N^2$. The parameters of the regression equations with 95% confidence bounds are given in the plots. The boxed data correspond to those that are boxed in figure 5.

5. Mixing efficiency

(a) Calculations of γ and its dependence on Re_b

The estimates of γ_χ and γ_f can be obtained from the regression plots $R_{m\chi}(Re_b)$ and $R_{mf}(Re_b)$ shown in figure 6*a*,*b*. According to (1.8), γ must be constant when R_m and Re_b are linearly dependent, which is satisfied for the regression $R_{m\chi}(Re_b)$ shown in figure 6*a* as

$$R_{m\chi} = \gamma_\chi Re_b, \quad \text{where } \gamma_\chi \approx 0.16. \tag{5.1}$$

For $R_{mf}(Re_b)$, however, the least-squared fit yields

$$R_{mf} = \xi (Re_b)^p \tag{5.2}$$

(figure 6*b*), where $\xi \approx 33$ is a non-dimensional regression coefficient and the exponent $p = 1/2$. The above leads to the Re_b dependence of

$$\gamma_{mf} = c_o \xi Re_b^{-1/2}. \tag{5.3}$$

In addition, γ_o, which is equivalent to γ_{mf}, was evaluated (table 1) using independent measurements of B and P, and the results are approximated in figure 7 as

$$\gamma_o = 50 Re_b^{-1/2}, \tag{5.4a}$$

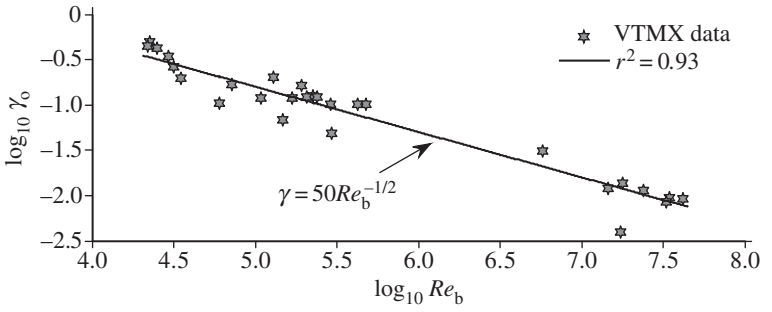

Figure 7. The mixing efficiency $\log_{10} \gamma_o$ (equations (1.6) and (1.7)) as a function of the buoyancy Reynolds number $\log_{10} Re_b$. The straight line is the least-squared approximation of the data by equation (5.2) with $c_o = 1.5$ (the 95% confidence bounds for c_o are 1.3 and 1.7); the coefficient of determination r^2 for the fit is given in the legend.

where $c_o \approx 1.5$. Note that the approximations (5.1), (5.2) and (5.4*a*) are obtained with high statistical confidence, with coefficients of determination $r^2 = 0.96$, 0.92 and 0.93, respectively.

At first glance, $\gamma_\chi \approx 0.16$ obtained in (5.1) for the nocturnal stably stratified atmospheric boundary layer is in good agreement with many previous estimates of γ for natural waters. In ocean mixing studies, $\gamma = 0.2$ is frequently used [4,14,54,56–63]; however, higher (up to 0.4) and lower (approx. 0.1) values of γ have also been suggested (e.g. [64] and [38,65,66]). Limnologists [13,67,68] usually prefer $\gamma = 0.15$–0.17, or in some cases, even smaller values, $\gamma = 0.04$–0.06 [69], at very low stabilities. Recent analysis of DNS data [15,25] showed an approximately linear regression between $R_{m\chi}$ and Re_b, also supporting $\gamma = 0.17$, but only in a relatively narrow range of $Re_b = 7$–10^2. The authors identified this range as a stationary transition turbulent regime sandwiched between decaying and developing turbulence.

Further, the direct numerical simulation (DNS) data [25] produced R_{mf} that appeared to be proportional to $2PrRe_b^{1/2}$ for $Re_b = 10^2$–10^3. This is identical to the functional dependence (5.3) shown in figure 6*b* based on our atmospheric dataset for much larger buoyancy Reynolds numbers, $Re_b > 10^3$, and therefore the dimensionless constant ξ is different. Results of several laboratory experiments [70–72] compiled in Shih *et al.* [25], together with DNS data, suggest that $R_m \sim Re_b^{1/3}$ (in our notation) when Re_b increases from 10^2 to 10^5. Note that the diffusivity in the laboratory experiments of Barry *et al.* [70] with grid-generated turbulence was calculated using the change of system's background potential energy before and after mixing events, and hence is an integral measure of different turbulent regimes. A slightly weaker than $Re_b^{1/2}$ dependence can be suggested for the eight most energetic ($\log_{10} Re_b > 6.5$) samples shown in figure 6*b* that can be approximated by a power function $R_{mf} \sim Re_b^{0.4}$. It is, however, reasonable to conclude that for the atmospheric nocturnal boundary layer $R_{mf} \sim Re_b^{1/2}$ for $Re_b > \approx 10^4$. The difference points to the sensitivity of γ to the calculation methods used as well as to the nature of the flow.

(b) Interdependence between R_{mf} and $R_{m\chi}$

In order to examine the disparity between the constant (equation (5.1)) and Re_b-dependent (equation (5.3)) mixing efficiencies evaluated using different methods, we analysed the relationship between mixing Reynolds numbers $R_{m\chi}$ and R_{mf} (figure 8). It appeared that 68 per cent of data in the plot occupy a relatively narrow range of intermediate values of $R_{m\chi}$ and R_{mf} (within the rectangle), wherein the linear regression $R_{mf} = c_R R_{m\chi}$ is valid with a relatively high coefficient of determination $r^2 = 0.64$ and a regression coefficient $c_R = 0.65$, having 95 per cent confidence bounds from 0.53 to 0.79. The deviation of c_R from the 'perfect agreement' case of $c_R = 1$ can be attributed to the uncertainties of evaluating ε and χ using Kolmogorov and Obukhov–Corrsin spectra, especially those associated with spectral constants c_{kw} and c_T in equation (3.1) and flux measurements.

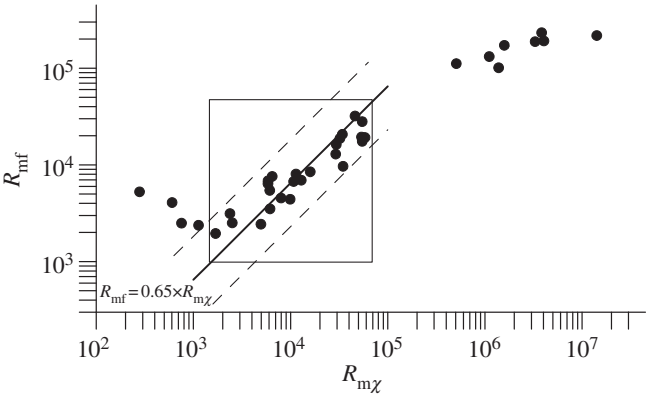

Figure 8. The mixing Reynolds number $R_{m\chi}$ (1.10*b*) versus R_{mf} (1.10*a*). The range where the linear regression $R_{mf} = 0.65 \times R_{m\chi}$ (straight line) is valid with the coefficient of determination $r^2 = 0.64$ enclosed in a rectangle. The dashed lines show the 95% confidence bounds of the regression. The data in the box are those that are also boxed in figures 5 and 6.

The difference between R_{mf} versus $R_{m\chi}$ is substantial at high and low ends of the R_m diagram, where approximately $10^6 < R_{m\chi} < 2 \times 10^7$ and $R_{mf} < (2\text{–}3) \times 10^5$. This is equivalent to high and low values of Re_b (figure 6*a*,*b*). Note, however, that large and small values of turbulent variables are usually subjected to highest uncertainties.

The striking loss of the parity between R_{mf} and $R_{m\chi}$ (or K_f and K_χ) at small and large Re_b invites explanation, which has a bearing on the estimation of fluxes in natural waters. Because $Re_b \sim (L_O/L_K)^{4/3}$, where $L_O = (\varepsilon/N^3)^{1/2}$ and $L_K = (\varepsilon/\nu^3)^{1/4}$ are the buoyancy (or Ozmidov) and Kolmogorov scales, respectively, $Re_b \gg 1$ implies very weakly stratified turbulence, where the TKE production essentially balances the dissipation, and fluxes are determined by r.m.s. velocity and temperature fluctuations ($\overline{w'T'} = c_\theta \overline{w'^2}^{1/2} \overline{T'^2}^{1/2}$, c_θ being a correlation coefficient [73]). This flux saturation, a reflection of a weak gradient or entraining fluid from non-turbulent regions, also implies non-stationarity and hence unsuitability of indirect methods of flux evaluation. On the other hand, small Re_b implies lack of the inertial subrange, which is essential for indirect flux estimation. A stationary balance between production of TKE, buoyancy flux and the rate of dissipation can be established only in a specific (figure 8) intermediate range of Re_b.

In other words, in fully developed turbulence at high $Re_b = 10^7\text{–}10^8$, a constant rate of mixing sustains until the density/temperature gradient almost completely erodes to a level that cannot uphold continuous growth of buoyancy (temperature) flux, whence the normalized diffusivity R_{mf} tends to saturation (compare the highest R_{mf} values in figures 5 and 6*b*). Less energetic turbulence ($Re_b < 10^4$) confounded by stratification produces weak mixing, which is characterized by the smallest $R_{mf} \approx (2\text{–}3) \times 10^3$. The results indicate that highly energetic (high Re_b) as well as underdeveloped (low Re_b) turbulence does not support stationary, non-diffusive and non-advective balance of Θ^2 in stratified flows. These findings are consistent with the interpretation of DNS data by Shih *et al.* [25]. The difference is the actual range of Re_b (a narrow one in both studies) where stationary turbulence prevails. The results can also be cast in terms of Ri, which is discussed below.

(c) Dependence of γ on Ri

The parametrization of mixing Reynolds number R_{mf} as a function of Ri given in §4 is a good representation for Richardson numbers below approximately 1. We have directly evaluated $\gamma_f \equiv \gamma_o$ (equation (1.6*a*) paired with equation (1.7)) and plotted it in figure 9 as a function of Ri. The growing trend of $\gamma_o(Ri)$ up to $Ri \approx 1$ seen here has been reported in several laboratory

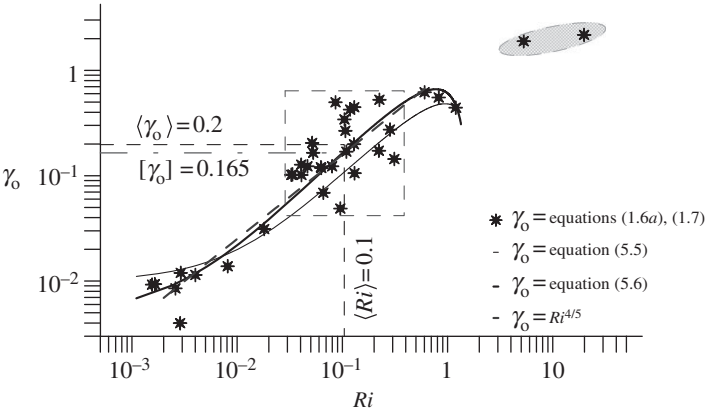

Figure 9. The mixing efficiency γ_o as a function of the Richardson number *Ri*. The polynomial approximations follow equations (5.4) and (5.5). The heavy dashed grey line is a nominal power $\gamma_o = Ri^{4/5}$. The data boxed in $0.03 < Ri < 0.4$ may represent, within scatter, an approximately constant mixing efficiency. The horizontal thin dashed lines show the box-averaged $\langle\gamma_o\rangle = 0.2$ and $\langle Ri\rangle = 0.1$, and the dash-dotted line is the box-median value of $[\gamma_o] = 0.165$. The shaded data correspond to the two samples in figure 5, which cannot be explained by local effects.

experiments, numerical and field studies [20,32,69,74–76]. Lozovatsky *et al.* [31] proposed an approximation,

$$\gamma_o = 0.01 + Ri - 0.53Ri^2, \tag{5.4}$$

to the GISS modelling results of Canuto *et al.* [36], in which the eddy coefficients are parametrized using specific damping functions. If we discard in figure 9 the two largest samples of γ_o corresponding to $Ri \gg 1$ as outliers (per discussion on two largest R_{mf} samples shown in figure 5 for $Ri > 4$), then the data trend broadly mimics equation (5.4), although the scatter is high. A better fit to this specific dataset is

$$\gamma_o = 0.005 + 1.7Ri - 1.1Ri^2, \tag{5.5}$$

which nicely captures the main trend shown in figure 9 by a bold line. The squared box in figure 9 encompasses the same range of *Ri* as that in figure 5 ($0.03 < Ri < 0.4$) and the corresponding range of R_m boxed in figures 6 and 8. The box-averaged mixing efficiency appeared to be equal $\langle\gamma_o\rangle = 0.2$, with the box-median value $[\gamma_o] = 0.165$. This is close to $\gamma = 0.16$ obtained using equations (1.8) and (1.12) in the $\log_{10} Re_b$ range 3.7–5.7 (figure 6*a*). The box-averaged Richardson number $\langle Ri\rangle = 0.1$ is smaller than the conventional critical value $Ri_{cr} = 0.25$, but still is in the range where shear-induced turbulence and internal mixing are dominant.

The above result can explain why a majority of microstructures in stratified oceans and lakes, where mixing is generated mainly by shear instabilities with *Ri* slightly below critical, leads to $\gamma = 0.16$–0.2 when evaluated using indirect methods (table 1). Note that atmospheric and laboratory measurements have spanned a wide range of *Ri* and Re_b, and hence exhibited significant variations of γ. A monotonic increase in γ_o with *Ri* can be seen from about 0.01 at $Ri \approx (2\text{–}3) \times 10^{-3}$ to 0.4–0.5 when *Ri* is approaching unity. However, in a limited range around *Ri* approximately 0.1, the mixing efficiency can be considered approximately constant close to 0.2. Note that in a weakly stratified upper oceanic layer, the median of *Ri* can be as low as 0.1 [31]. The cumulative distribution of the Richardson number is often well approximated by a lognormal probability law, showing that the probability of $Ri < 0.25$ can be above 60 per cent and for $Ri < 1$, can approach 80 per cent.

Considering that two variables *Ri* and Re_b are involved in determining fluxes (§2), we plot contours of $\gamma_o(Ri, Re_b)$ in figure 10, which show that γ_o in the boxed area (*Ri* and Re_b range associated with shear-generated turbulence) is between 0.1 and approximately 0.3. On the basis of our data, the upper cut-off Re_b^{up} was identified as approximately 5×10^5 ($Ri < 0.4$), beyond

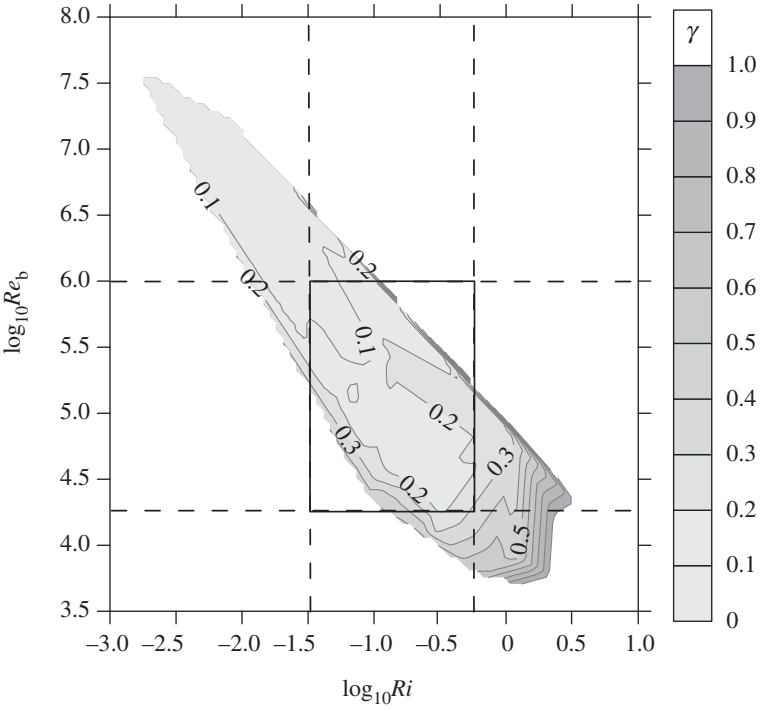

Figure 10. The contour plot of mixing efficiency γ_o as a function of Ri and Re_b. The rectangle confines the same range of Ri and Re_b as in figures 8 and 9.

which buoyancy effects are insignificant, whereas the lower limit was $Re_b^{lw} \approx 10^4$ $(Ri > 0.03)$, signifying the absence of a clear inertial subrange due to suppression of local production of TKE. The variability of γ_o outside this $Ri - Re_b$ range is possibly due to other types of TKE sources unrelated to mean shear and/or to non-stationary turbulence (developing at $Ri < 0.03$, $Re_b > \sim 10^6$ or decaying at $Ri > 0.3$, $Re_b < 10^4$).

6. Discussion and conclusions

Vertical heat, mass and momentum fluxes have not been directly measured in oceans and lakes until recently, and thus the eddy viscosity and diffusivities that are central to predictive modelling are inferred indirectly. One method relies on the assumption that the mixing efficiency γ is a constant in the expression $K_T N^2 = \gamma\varepsilon$. Alternatively, a simplified scalar balance equation $K_T(\partial\tilde{T}/\partial z)^2 = \chi/2$ is used. The possible variability of γ was investigated in this paper based on sonic anemometer data obtained from the stable atmospheric boundary layer. The diffusivity $K_T \equiv K_f$ and the corresponding mixing Reynolds number R_{mf} (equation (1.10*a*) and table 1) were evaluated using temperature flux and gradient measurements and ε via the kinetic energy spectra; γ so obtained was designated as $\gamma = \gamma_f$. The results were compared with $\gamma = \gamma_x$, which was evaluated using $K_T \equiv K_\chi$ and the corresponding $R_{m\chi}$ (equation (10*b*)) based on the commonly used (in physical oceanography) scalar dissipation technique (equation (1.12)). Dimensional arguments suggest that, at high buoyancy Reynolds numbers Re_b, γ is a function of Ri and Re_b, but the dependence on molecular parameters such as Pr is negligibly weak [25].

It was found that $\gamma \approx 0.16$ is nominally a constant in the range $10^4 < Re_b < 10^6$, and for our data, this corresponds to approximately $0.03 < Ri < 0.4$. Both normalized diffusivities R_{mf} and $R_{m\chi}$ coincide in this regime (figures 5 and 8), leading to $R_m \sim Ri^{-3/2}$, indicating an approximate equivalence between γ_f and γ_x. Outside the above parameter ranges, R_m can be parametrized as

a function of Ri using equation (4.1). For very low and high Re_b and Ri, the basic assumptions underlying $K_T N^2 = \gamma\varepsilon$ were untenable, and should be used with circumspection. Furthermore, the accuracy of measurements, calibration of sensors as well as the usage of Obukhov–Corrsin spectral forms all affect the numerical value of γ.

The mixing efficiency was found to be a growing function of Ri (equation (5.5)) in a wide range, $0.002 < Ri < 1$. It was a decreasing function of Re_b, according to $\gamma \sim Re_b^{-1/2}$ (equation (5.3)), in the range $3 \times 10^4 < Re_b < 3 \times 10^7$, which is in agreement with the DNS results of Shih *et al.* [25] for $10^2 < Re_b < 10^3$, but at odds with Gargett's [77] suggestion of $\gamma \sim Re_b^{-1}$ for approximately the same range of Re_b (based on laboratory data of Itsweire *et al.* [78]). If turbulence is anisotropic at smaller Reynolds numbers, as argued by Gargett [77], then it impacts the dissipation estimates and hence mixing efficiency calculations. Detailed studies on the dependence of γ with Ri and Re_b were not possible, given the difficulty of obtaining γ versus Ri and Re_b in nature when one or the other parameter is constant (equation (2.1)). The mixing efficiency may vary from approximately 0.01 at $Ri \approx (2\text{–}3) \times 10^{-3}$ to approximately 0.5–0.6 at $Ri \sim 1$. Phillips [33] suggested an increase of Ri up to a critical value Ri_0, following a γ decrease at higher Ri. This trend was implemented by Canuto *et al.* [36] in modelling, and was experimentally observed by Strang & Fernando [22], Guyez *et al.* [79] and others. A decrease in γ at high Ri was evident (figure 9 and equation (5.5)), but could not be confirmed using the present dataset, as in the case of stably stratified Arctic boundary-layer data presented by Grachev *et al.* [80,81]. In our case, the number of high Ri data points are only a handful, thus precluding any inferences.

At Richardson numbers close to or below a critical value $Ri_{cr} \sim 0.1\text{–}0.25$ (viz. approx. $0.03 < Ri < 0.4$), direct measurements of $\gamma = \gamma_o$ via fluxes and gradients could be approximately treated as a constant with a characteristic value between 0.16 and 0.2. This Ri range is most pertinent to shear-generated stratified turbulent layers of oceans and lakes, which may explain why γ is often observed to be close to 0.2 and treated as such [82]. In this range, the microstructure-based estimates γ_x and γ_f are consistent with γ_o, showing $\gamma \approx 0.16$. Comparison of different observations, nonetheless, is stymied by the dependence of Ri on measurement resolution, in particular, the separation with which the gradients are estimated. DeSilva *et al.* [83] showed that when this separation is greater than the buoyancy scale, the measurement may not be representative of local Ri, and our data were on the verge of this limit.

Our results help shed light on the differences between mixing efficiencies often encountered in oceanographic and limnological studies. Both constant and variable values of mixing efficiency are used, which forms the basis of closure in numerical models [84]. The present results show that a constant mixing efficiency can be used only in a limited range of governing parameters (Ri, Re_b), and many oceanographic measurements appear to be in this range [85]; therein turbulence is internally generated and approximately satisfies conditions of stationarity and homogeneity.

We are thankful to the participants of the VTMX experiment who conducted the field measurements and to Andrea Dato (a former student of University of Rome 'La Sapienza', Italy) who actively participated in the data processing during his visit to the USA. This work was supported by the National Science Foundation (CMG) and ONR grants nos N00014-10-1-0738 and N00014-11-1-0709 (MATERHORN Programme).

References

1. Monin AS, Yaglom AM. 1975 *Statistical fluid mechanics: mechanics of turbulence*, vol. 2. Cambridge, MA: MIT Press.
2. Turner JS. 1981 Small-scale mixing processes. In *Evolution of physical oceanography* (eds BA Warren, C Wunsch), pp. 236–262. Cambridge, MA: MIT Press.
3. Gregg MC. 1989 Scaling turbulent dissipation in the thermocline. *J. Geophys. Res.* **94**, 9686–9698. (doi:10.1029/JC094iC07p09686)
4. Oakey NS. 1982 Determination of the rate of dissipation of turbulent energy from simultaneous temperature and velocity shear microstructure measurements. *J. Phys. Oceanogr.* **12**, 256–271. (doi:10.1175/1520-0485(1982)012<0256:DOTROD>2.0.CO;2)

5. Moum JN, Gregg M, Licen C, Carr ME. 1995 Comparison of turbulence kinetic energy dissipation rate estimates from two ocean microstructure profiler. *J. Atmos. Oceanic Technol*. **12**, 346–365. (doi:10.1175/1520-0426(1995)012<0346:COTKED>2.0.CO;2)
6. Prandke H, Stips A. 1998 Test measurements with an operational microstructure turbulence profiler: detection limit of dissipations rates. *Aquatic Sci*. **60**, 191–209. (doi:10.1007/s000270050036)
7. Paka VT, Nabatov VN, Lozovatsky ID, Dillon TM. 1999 Ocean microstructure measurements by BAKLAN and GRIF. *J. Atmos. Oceanic Technol*. **16**, 1519–1532. (doi:10.1175/1520-0426(1999)016<1519:OMMBBA>2.0.CO;2)
8. Wolk F, Yamazaki H, Seuront L, Lueck RG. 2002 A new free-fall profiler for measuring biophysical microstructure. *J. Atmos. Oceanic Technol*. **19**, 780–793. (doi:10.1175/1520-0426(2002)019<0780:ANFFPF>2.0.CO;2)
9. Lueck RL, Lu Y. 1997 The logarithmic layer in a tidal channel. *Continental Shelf Res.* **17**, 1785–1801. (doi:10.1016/S0278-4343(97)00049-6)
10. Souza AJ, Howarth MJ. 2005 Estimates of Reynolds stress in highly energetic shelf sea. *Ocean Dyn.* **55**, 490–498. (doi:10.1007/s10236-005-0012-7)
11. Lozovatsky I, Roget E, Planella J, Fernando HJS, Liu Z. 2010 Intermittency of near-bottom turbulence in tidal flow on a shallow shelf. *J. Geophys. Res*. **115**, C05006. (doi:10.1029/2009JC005325)
12. Lozovatsky I, Liu Z, Fernando HJS, Armengol J, Roget E. 2011 Shallow water tidal currents in close proximity to the seafloor and boundary-induced turbulence. *Ocean Dyn.* (doi:10.1007/s10236-011-0495-3)
13. Ivey GN, Imberger J. 1991 On the nature of turbulence in a stratified fluid. I. The energetics of mixing. *J. Phys. Oceanogr*. **21**, 650–658. (doi:10.1175/1520-0485(1991)021<0650:OTNOTI>2.0.CO;2)
14. Osborn TR. 1980 Estimates of the local rate of vertical diffusion from dissipation measurements. *J. Phys. Oceanogr*. **10**, 83–89. (doi:10.1175/1520-0485(1980)010<0083:EOTLRO>2.0.CO;2)
15. Ivey GN, Winters KB, Koseff JR. 2008 Density stratification, turbulence, but how much mixing? *Annu. Rev. Fluid Mech*. **40**, 169–184. (doi:10.1146/annurev.fluid.39.050905.110314)
16. Fernando HJS. 1991 Turbulent mixing in stratified fluids. *Annu. Rev. Fluid Mech*. **23**, 455–493. (doi:10.1146/annurev.fl.23.010191.002323)
17. Peltier WR, Caulfield CP. 2003 Mixing efficiency in stratified shear flows. *Annu. Rev. Fluid Mech*. **35**, 135–167. (doi:10.1146/annurev.fluid.35.101101.161144)
18. Linden PF. 1979 Mixing in stratified fluids. *Geophys. Astrophys. Fluid Dyn*. **13**, 3–23. (doi:10.1080/03091927908243758)
19. Rohr JJ, Itsweire EC, Van Atta CW. 1984 Mixing efficiency in stably stratified decaying turbulence. *Geophys. Astrophys. Fluid Dyn*. **29**, 221–236. (doi:10.1080/03091928408248190)
20. Rohr J, Van Atta C. 1987 Mixing efficiencies in stably stratified growing turbulence. *J. Geophys. Res.* **92**, 5481–5488. (doi:10.1029/JC092iC05p05481)
21. Monti P, Querzoli G, Cenedese A, Piccinini S. 2007 Mixing properties of a stably stratified parallel shear layer. *Phys. Fluids* **19**, 085104. (doi:10.1063/1.2756580)
22. Strang EJ, Fernando HJS. 2001 Entrainment and mixing in stratified shear flows. *J. Fluid Mech*. **428**, 349–386. (doi:10.1017/S0022112000002706)
23. McEwan AD. 1983 Internal mixing in stratified fluids. *J. Fluid Mech*. **128**, 59–80. (doi:10.1017/S0022112083000385)
24. Smyth WD, Moum JN, Caldwell DR. 2001 The efficiency of mixing in turbulent patches: inferences from direct simulations and microstructure observations. *J. Phys. Oceanogr*. **31**, 1969–1992. (doi:10.1175/1520-0485(2001)031<1969:TEOMIT>2.0.CO;2)
25. Shih LH, Koseff JR, Ivey GN, Ferziger JH. 2005 Parameterization of turbulent fluxes and scales using homogenous sheared stably stratified turbulence simulations. *J. Fluid Mech*. **525**, 193–214. (doi:10.1017/S0022112004002587)
26. Joseph B, Mahalov A, Nicolaenko B, Tse KL. 2004 Variability of turbulence and its outer scales in a model tropopause jet. *J. Atmos. Sci*. **61**, 621–643. (doi:10.1175/1520-0469(2004)061<0621:VOTAIO>2.0.CO;2)
27. St. Laurent L, Schmitt RW. 1999 The contribution of salt fingers to vertical mixing in the North Atlantic trace release experiment. *J. Phys. Oceanogr*. **29**, 1404–1424. (doi:10.1175/1520-0485(1999)029<1404:TCOSFT>2.0.CO;2)

28. Wijesekera HW, Dillon TM. 1997 Shannon entropy as an indicator of age for turbulent overturns in the oceanic thermocline. *J. Geophys. Res.* **102**, 3279–3291. (doi:10.1029/96JC03605)
29. Lozovatsky ID. 1996 Turbulence decay in stratified and homogeneous marine layers. *Dyn. Atmos. Oceans* **24**, 15–25. (doi:10.1016/0377-0265(95)00407-6)
30. Prastowo T, Griffiths RW, Hughes GO, Hogg AM. 2009 Effects of topography on the cumulative mixing efficiency in exchange flows. *J. Geophys. Res.* **114**, C08008. (doi:10.1029/2008JC005152)
31. Lozovatsky I, Roget E, Fernando HJS, Figueroa M, Shapovalov S. 2006 Sheared turbulence in a weakly-stratified upper ocean. *Deep-Sea Res. I* **53**, 387–407. (doi:10.1016/j.dsr.2005.10.002)
32. Balmforth NJ, Llewellyn Smith SG, Young WR. 1998 Dynamics of interface and layers in a stratified turbulent fluid. *J. Fluid Mech.* **355**, 329–358. (doi:10.1017/S0022112097007970)
33. Phillips OM. 1972 Turbulence in a strongly stratified fluid: is it unstable? *Deep-Sea Res.* **19**, 79–81. (doi:10.1016/0011-7471(72)90074-5)
34. Linden PF. 1980 Mixing across a density interface produced by grid turbulence. *J. Fluid Mech.* **100**, 691–703. (doi:10.1017/S002211208000136X)
35. Pardyjak ER, Monti P, Fernando HJS. 2002 Flux Richardson number measurements in stable atmospheric shear flows. *J. Fluid Mech.* **459**, 307–316. (doi:10.1017/S0022112002008406)
36. Canuto VM, Howard A, Cheng Y, Dubovikov MS. 2001 Ocean turbulence. Part I: One-point closure model—momentum and heat vertical diffusivities. *J. Phys. Oceanogr.* **31**, 1413–1426. (doi:10.1175/1520-0485(2001)031<1413:OTPIOP>2.0.CO;2)
37. Gargett AE, Moum JN. 1995 Mixing efficiencies in turbulent tidal fronts: results from direct and indirect measurements of density flux. *J. Phys. Oceanogr.* **25**, 2583–2608. (doi:10.1175/1520-0485(1995)025<2583:MEITTF>2.0.CO;2)
38. Moum JN. 1996 Efficiency of mixing in the main thermocline. *J. Geophys. Res.* **101**, 12 057–12 069. (doi:10.1029/96JC00508)
39. Jacobitz FG, Sarkar S. 1999 On the shear number effect in stratified shear flow. *Theor. Comput. Fluid Dyn.* **13**, 171–188. (doi:10.1007/s001620050114)
40. Esau I, Grachev A. 2007 Turbulent Prandtl number in stably stratified atmospheric boundary layer: intercomparison between LES and SHEBA data. *e-WINDENG* (005), 1–17. See http://ejournal.windeng.net.
41. Elliott Z, Venayagamoorthy SK. 2011 Evaluation of turbulent Prandtl (Schmidt) number parameterizations for stably stratified environmental flows. *Dyn. Atmos. Oceans* **51**, 137–150. (doi:10.1016/j.dynatmoce.2011.02.003)
42. Lee S-M, Giori W, Princevac M, Fernando HJS. 2006 Implementation of a stable PBL turbulence parameterization for the mesoscale model MM5: nocturnal flow in complex terrain. *Bound.-Layer Meterol.* **119**, 109–134. (doi:10.1007/s10546-005-9018-4)
43. Monti P, Fernando HJS, Chan WC, Princevac M, Kowalewski TA, Pardyjak E. 2002 Observations of flow and turbulence in the nocturnal boundary layer over a slope. *J. Atmos. Sci.* **59**, 2513–2534. (doi:10.1175/1520-0469(2002)059<2513:OOFATI>2.0.CO;2)
44. Princevac M, Hunt JCR, Fernando HJS. 2008 Quasi-steady katabatic winds on slopes in wide valleys: hydraulic theory and observations. *J. Atmos. Sci.* **65**, 627–643. (doi:10.1175/2007JAS2110.1)
45. Pope SB. 2000 *Turbulent flows*. Cambridge, UK: Cambridge University Press.
46. Sreenivasan KR. 1996 The passive scalar spectrum and the Obukhov–Corrsin constant. *Phys. Fluids* **8**, 189–196. (doi:10.1063/1.868826)
47. Turner JS. 1986 Turbulent entrainment: the development of the entrainment assumption, and its application to geophysical flows. *J. Fluid Mech.* **173**, 431–471. (doi:10.1017/S0022112086001222)
48. Pelegri JL, Csanady GT. 1994 Dyapycnal mixing in western boundary currents. *J. Geophys. Res.* **99**, 18 275–18 304. (doi:10.1029/94JC01201)
49. Munk WH, Anderson ER. 1948 Notes on the theory of the thermocline. *J. Mar. Res.* **3**, 276–295.
50. Jones JH. 1973 Vertical mixing in equatorial undercurrent. *J. Phys. Oceanogr.* **3**, 286–296. (doi:10.1175/1520-0485(1973)003<0286:VMITEU>2.0.CO;2)
51. Ueda H, Mitsumoto S, Komori S. 1981 Buoyancy effects on the turbulent transport processes in the lower atmosphere. *Q. J. R. Meteorol. Soc.* **107**, 561–578. (doi:10.1256/smsqj.45306)
52. Pacanowski RC, Philander SGH. 1981 Parameterization of vertical mixing in numerical models of tropical oceans. *J. Phys. Oceanogr.* **11**, 1443–1451. (doi:10.1175/1520-0485(1981)011<1443:POVMIN>2.0.CO;2)

53. Henderson-Sellers B. 1982 A simple formula for vertical eddy diffusion coefficients under conditions of non-neutral stability. *J. Geophys. Res*. **87**, 5860–5864. (doi:10.1029/JC087iC08p05860)
54. Peters H, Gregg MC, Tool JM. 1988 On the parameterization of equatorial turbulence. *J. Geophys. Res*. **93**, 1199–1218. (doi:10.1029/JC093iC02p01199)
55. Soloviev A, Lukas R, Hacker P. 2001 An approach to parameterization of the oceanic turbulent boundary layer in the western Pacific warm pool. *J. Geophys. Res*. **106**, 4421–4435. (doi:10.1029/2000JC900154)
56. Gregg M, D'Asaro E, Shay T, Larson N. 1986 Observations of persistent mixing and near-inertial internal waves. *J. Phys. Oceanogr*. **16**, 856–885. (doi:10.1175/1520-0485(1986)016<0856:OOPMAN>2.0.CO;2)
57. Moum JN, Osborn TR, Paulson CA. 1989 Mixing in the equatorial surface layer. *J. Geophys. Res*. **94**, 2005–2021. (doi:10.1029/JC094iC02p02005)
58. Ruddick B, Walsh D, Oakey N. 1997 Variations in apparent mixing efficiency in the North Atlantic Central Water. *J. Phys. Oceanogr*. **27**, 2589–2605. (doi:10.1175/1520-0485(1997)027<2589:VIAMEI>2.0.CO;2)
59. Lozovatsky ID, Dillon TM, Erofeev AYu, Nabatov VN. 1999 Variations of thermohaline structure and turbulent mixing on the Black Sea shelf at the beginning of autumn cooling. *J. Mar. Syst*. **21**, 255–282. (doi:10.1016/S0924-7963(99)00018-4)
60. Finnigan TD, Luther DS, Lukas R. 2002 Observations of enhanced diapycnal mixing near the Hawaiian Ridge. *J. Phys. Oceanogr*. **32**, 2988–3002. (doi:10.1175/1520-0485(2002)032<2988:OOEDMN>2.0.CO;2)
61. Lozovatsky ID, Fernando HJS. 2002 Mixing on a shallow shelf of the Black Sea. *J. Phys. Oceanogr*. **32**, 945–956. (doi:10.1175/1520-0485(2002)032<0945:MOASSO>2.0.CO;2)
62. Rippeth TP, Inall ME. 2002 Observations of the internal tide and associated mixing across the Malin Shelf. *J. Geophys. Res*. **107**, 3028. (doi:10.1029/2000JC000761)
63. Oakey NS, Greenan BJW. 2004 Mixing in a coastal environment. II. A view from microstructure measurements. *J. Geophys*. Res. **109**, C10014. (doi:10.1029/2003jc002193)
64. Moum JN. 1990 The quest for K_ρ: preliminary results from direct measurements of turbulent fluxes in the ocean. *J. Phys. Oceanogr*. **20**, 1980–1984. (doi:10.1175/1520-0485(1990)020<1980:TQFRFD>2.0.CO;2)
65. Arneborg L. 2002 Mixing efficiencies in patchy turbulence. *J. Phys. Oceanogr*. **32**, 1496–1506. (doi:10.1175/1520-0485(2002)032<1496:MEIPT>2.0.CO;2)
66. Fringer OB, Street RL. 2003 The dynamics of breaking progressive interfacial waves. *J. Fluid Mech*. **494**, 319–353. (doi:10.1017/S0022112003006189)
67. Imberger J. 1994 Transport processes in lakes: a review. In *Limnology now: a paradigm of planetary problems* (ed. R Margalef), pp. 99–193. New York, NY: Elsevier.
68. Wuest A, Lorke A. 2003 Small-scale hydrodynamics in lakes. *Annu. Rev. Fluid Mech*. **35**, 373–412. (doi:10.1146/annurev.fluid.35.101101.161220)
69. Etemad-Shahidi A, Imberger J. 2002 Anatomy of turbulence in a narrow and strongly stratified estuary. *J. Geophys. Res*. **107**, 3070. (doi:10.1029/2001JC000977)
70. Barry ME, Ivey GN, Winters KB, Imberger J. 2001 Measurements of diapycnal diffusivities in stratified fluids. *J. Fluid Mech*. **442**, 267–291. (doi:10.1017/S0022112001005080)
71. Jackson PR, Rehmann CR. 2003 Laboratory measurements of differential diffusion in a diffusively stable, turbulent flow. *J. Phys. Oceanogr*. **33**, 1592–1603. (doi:10.1175/2405.1)
72. Rehmann CR, Koseff JR. 2004 Mean potential energy change in stratified grid turbulence. *Dyn. Atmos. Oceans* **37**, 271–294. (doi:10.1016/j.dynatmoce.2003.09.001)
73. Sreenivasan KR, Tavoularis S, Henry R, Corrsin S. 1980 Temperature fluctuations and scales in grid-generated turbulence. *J. Fluid Mech*. **100**, 597–621. (doi:10.1017/S0022112080001309)
74. Strang EJ, Fernando HJS. 2001 Vertical mixing and transports through a stratified shear layer. *J. Phys. Oceanogr*. **31**, 2026–2048. (doi:10.1175/1520-0485(2001)031<2026:VMATTA>2.0.CO;2)
75. Saggio A, Imberger J. 2001 Mixing and turbulent fluxes in the metalimnion of a stratified lake. *Limnol. Oceanogr*. **46**, 392–409. (doi:10.4319/lo.2001.46.2.0392)
76. Peters H, Bokhorst R. 2001 Microstructure observations of turbulent mixing in a partially mixed estuary. II. salt flux and stress. *J. Phys. Oceanogr*. **93**, 1105–1109. (doi:10.1175/1520-0485(2001)031<1105:MOOTMI>2.0.CO;2)
77. Gargett A. 1988 The scaling of turbulence in the presence of stable stratification. *J. Geophys. Res*. **93**(C5), 5021–5036. (doi:10.1029/JC093iC05p05021)

78. Itsweire EC, Helland KN, Van Atta CW. 1986 The evolution of grid-generated turbulence in a stably stratified fluid. *J. Fluid Mech*. **162**, 299–338. (doi:10.1017/S0022112086002069)
79. Guyez EJ, Fl'or JB, Hopfinger EJ. 2007 Turbulent mixing at a stable density interface: the variation of the buoyancy flux-gradient relation. *J. Fluid Mech*. **577**, 127–136. (doi:10.1017/S0022112007004958)
80. Grachev AA, Fairall CW, Persson POG, Andreas EL, Guest PS. 2005 Stable boundary-layer scaling regimes: the SHEBA data. *Bound.-Layer Metereol*. **116**, 201–235. (doi:10.1007/s10546-004-2729-0)
81. Grachev AA, Andreas EL, Fairall CW, Guest PS, Persson POG. 2008 Turbulent measurements in the stable atmospheric boundary layer during SHEBA: ten years after. *Acta Geophys.* **56**, 142–166. (doi:10.2478/s11600-007-0048-9)
82. Gregg MC, Alford MH, Kontoyiannis H, Zervakis V, Winkel D. 2012 Mixing over the steep side of the Cycladic Plateau in the Aegean Sea. *J. Mar. Syst*. **89**, 30–47. (doi:10.1016/j.jmarsys.2011.07.009)
83. DeSilva IPD, Brandt A, Montenegro L, Fernando HJS. 1999 Gradient Richardson number measurements in stratified shear layers. *Dyn. Atmos. Oceans* **30**, 47–68. (doi:10.1016/S0377-0265(99)00015-9)
84. Zaron ED, Moum JN. 2009 A new look at Richardson number mixing schemes for equatorial ocean modeling. *J. Phys. Oceanogr*. **39**, 2652–2664. (doi:10.1175/2009JPO4133.1)
85. Kundu PK, Beardsley RC. 1991 Evidence of a critical Richardson number in moored measurements during the upwelling season off Northern California. *J. Geophys. Res*. **96**, 4855–4868. (doi:10.1029/90JC02108)